5G New Radio LDPC Codes Based Generalized Joint Subcarrier-Time Index Modulation DCSK System

Muntaha K. Musa* and Fadhil S. Hasan
Faculty of Engineering, Mustansiriyah University, Baghdad, Iraq
Email: muntaha.kadhum@uomustansiriyah.edu.iq (M.K.M.), fadel_sahib@uomustansiriyah.edu.iq (F.S.H.)

Manuscript received June 13, 2025; revised July 30, 2025; accepted August 16, 2025
*Corresponding author

***Abstract*—Low-Density-Parity-Check (LDPC) codes are a cornerstone for achieving robust error correction capabilities in 5G New Radio applications, significantly improving the reliability of data transmission across noisy and unpredictable wireless channels. Since an evaluation and discussion of the performance with channel coding is significantly absent in two-dimensional Index Modulation (IM)-Differential Chaos Shift Keying (DCSK) schemes. Therefore, in this study, the 5G new radio LDPC codes based generalized joint subcarrier-time index modulation DCSK system (5G NR-LDPC-GJSTIM-DCSK) is proposed, where 5G NR-LDPC codes are used as channel coding. The aim is to improve the system's performance specifically across AWGN (additive white gaussian noise) and multipath Rayleigh fading channels, when contrasted with the uncoded GJSTIM-DCSK. In the suggested system, the detected index bits at the receiver are transformed into soft bits and combined with the soft demodulated bits before the decoding process. The results show that the highest coding improvements are 11.6 dB for AWGN channels and 22.2 dB for Rayleigh fading channels, using a code rate of 1/5, a codeword length of 7648, and a spreading factor of 256. Additionally, the performance of the 5G NR-LDPC-GJSTIM-DCSK system surpasses the 5G NR-LDPC-GSIM-DCSK-II's performance and is nearly equivalent to the 5G NR-LDPC-GFTIM-DCSK-II's performance at high SNR (Signal to Noise Ratio).**

***Index Terms*—5G new radio Low-Density-Parity-Check (LDPC), differential chaos shift keying, joint subcarrier-time index modulation, multipath Rayleigh fading channel**

I. Introduction

The non-coherent Differential Chaos Shift Keying (DCSK) scheme [1], which utilizes chaotic signals for spread spectrum transmission, is among the most extensively studied digital communication schemes. They have garnered significant research interest due to their inherent advantage of eliminating the requirement for a synchronized chaotic signal replica at the receiver. Generating such a replica can be a complex task, particularly in high-noise environments.

Consequently, numerous studies have been presented, aiming to address the inherent limitations of DCSK, primarily its low data rate and poor spectral efficiency [2, 3].

M-ary implementations of DCSK and CS-DCSK (code shift-DCSK) were presented [4, 5]. These works integrated various novel approaches aimed at improving both the data throughput and energy efficiency of these systems.

Additionally, Lu, Mohammed *et al*. [6, 7] explored innovative techniques to enhance DCSK system performance regarding Bit Error Rate (BER) and noise reduction. For instance, Lu *et al*. [6] employed reference diversity, transmitting multiple copies of the reference signal to mitigate channel noise interference. Concurrently, the work in [7] leveraged the security benefits of frequency hopping in conjunction with New Radio (NR)-DCSK's noise mitigation features.

Following the development of Index Modulation (IM), several studies have explored its integration with DCSK modulation, as demonstrated in [8] and [9]. These works presented techniques that utilize the index of one transmitter resource (carrier index) in various ways to convey additional bits. This approach effectively expands the information rate, energy efficiency, and spectrum efficiency of these systems without increasing bandwidth or energy consumption.

Two-dimensional index modulation (involving subcarriers and time slots, or distinct permutations) was combined with DCSK modulation through different approaches to further enhance transmitted information rate, spectral efficiency, and energy efficiency [10–13].

A Generalized Joint Subcarrier-Time Index Modulation (GJSTIM) based on DCSK was proposed. In this system, extra bits were sent using the indices of subcarriers and time slots, picking them out using a method called combinatorial mapping [14]. Additionally, this approach used a clever grouping technique, splitting all subcarriers into 'G' groups. Each group then sent out its index bits and DCSK-modulated bits, with those modulated bits going across all the active subcarrier time slots and even through unselected time slots in idle subcarriers. This entire setup enhanced the data rate compared to earlier two-dimensional index modulation DCSK systems [10–13], and improved spectral and energy efficiency. Furthermore, by incorporating some noise reduction techniques and a Hilbert transform, the system managed to boost BER performance compared to other DCSK index modulation systems.

doi: 10.18178/ijeetc.14.5.253-265

Recently, DCSK systems employing several dimensions of index modulation (three, four, and five dimensions) were developed in [15–17] to significantly enhance data rate and spectral efficiency. Specifically, Hasan and Valenzuela [15] employed subcarrier, time, and reference indices to enhance the data rate. In contrast, Zhang *et al*. [16] utilized the indices of four-dimensional index modulation (subcarrier, time, Walsh code, and sorting indices) to transmit additional bits, hence attaining favorable spectral efficiency. Moreover, Hasan [17] expanded the variety of resource types utilized in index modulation to five indices (subcarrier, time, Walsh code, reference permutation, and Walsh code permutation) to develop an ultra-high transmission rate system. Despite these developments in data rate, there was a concomitant increase in system complexity.

Consequently, ensuring high reliability and lower power consumption significantly influences the efficacy of wireless communication systems; therefore, numerous researchers incorporate channel coding, such as Low-Density Parity Check (LDPC) codes, into DCSK systems to enhance reliability and mitigate the BER of transmitted data.

In this context, for transmission systems seeking a favorable compromise between power consumption and spectral efficiency, coded modulation provides an effective solution. It facilitates significant coding advantages without incurring bandwidth overhead.

To achieve superior DCSK performance approaching its theoretical capacity, Coded Modulation (CM) was employed in [18]. This work investigated the integration of two novel non-binary protograph-LDPC codes with M-ary-DCSK modulation, utilizing an Extrinsic Information Transfer (EXIT) method. The performance was evaluated across a Rayleigh fading channel. Notably, the CM-DCSK approach simplifies receiver design compared to DC-BICM (differentially chaos bit-interleaved coded modulation) by eliminating the need for iterative processing connecting the non-coherent receiver and the channel decoder.

Subsequently, the performance of both uncoded and coded DCSK systems in Additive White Gaussian Noise (AWGN) environments was investigated in [19], utilizing four distinct types of LDPC decoders. Simulation results demonstrated a performance improvement of 1.3 to 4.6 dB, with the log-domain decoder showing superior performance compared to the other three decoders.

Mosleh, Hasan, and Abdulhameed [20] implemented an LDPC-coded DCSK system using a Xilinx Kintex-7 FPGA development kit. Their investigation focused on characterizing the hardware efficiency and resource utilization characteristics of this system, specifically examining the impact of the min-sum decoding algorithm over an AWGN channel.

Further expanding on coding techniques, Xu *et al*. [21] investigated a protograph-LDPC coded DC-BICM system within the context of Underwater Acoustic (UWA) communication. This work also presented a novel short-length protograph-LDPC code methodology for DC-BICM that incorporated the DC-BICM system, an Underwater Acoustic (UWA) channel model, and a differential evolution search algorithm to optimize the code. Through simulations, the protograph-LDPC code proposed in [21] demonstrated superior performance over conventional codes regarding both error correction ability and rapid convergence. Moreover, evaluations of underwater image transmission also indicated that this code achieved superior image quality, as evidenced by higher PSNR values.

An enhanced decoder architecture was presented for the M-ary-protograph coded DCSK, which utilized a unique Initial Chaotic Signal Estimation (ICSE) method [22]. This development was crucial because the conventional M-ary DCSK decoder inadequately exploited the data embedded in redundant chaotic sequences. In the system proposed in [22], data from each redundant chaotic sequence was employed to ascertain the original chaotic sequence, thereby yielding a precise Log-Likelihood-Ratio (LLR) and enhancing error performance. Furthermore, a unique protograph code was developed to enhance system performance utilizing the Protograph Extrinsic Information Transfer (P-EXIT) technique.

Taking these advancements further, a team in [23] introduced a Coded Grouping Subcarrier-Index Modulation-Differential Chaos Shift Keying (CGSIM-DCSK) system employing suite-coded modulation to boost BER performance across a multipath fading channel. This system involved converting the detected subcarrier index bits at the receiver into a bipolar format prior to the channel decoding process, while incorporating the soft-modulated bits. Their method integrated two types of channel coding with both GSIM-DCSK schemes: LDPC code and 5G NR-Polar code. Simulation results demonstrated that the LDPC code exhibited marginally superior performance compared to the 5G NR-polar code when tested on a multipath Rayleigh fading channel.

Previous studies haven't explored combining two-dimensional IM-aided DCSK with 5G NR-LDPC codes, even though each has been individually successful in DCSK systems. This research investigates the potential benefits of integrating these coding techniques within GJSTIM-DCSK modulation to enhance overall performance. Specifically, we examine how these robust error correction methods, paired with two-dimensional index modulation, can enhance the efficiency and reliability of Telecommunication systems.

Herein, we present our suggested 5G NR-LDPC-GJSTIM-DCSK system. It attains exceptional performance chiefly by synergistically integrating the robust error-correction capabilities of 5G NR-LDPC codes with the improved spectrum and energy efficiency provided by generalized joint subcarrier-time index modulation. This utilizes the inherent robustness of differential chaos shift keying. Specifically, the incorporation of 5G NR-LDPC codes guarantees near-capacity error performance, which is essential for current wireless standards. Furthermore, GJSTIM-DCSK

significantly enhances spectrum efficiency by transmitting information not only by conventional symbol modulation but also through the smart selection of active subcarrier-time indices, resulting in increased data throughput. DCSK's non-coherent reception inherently offers robust resilience against multipath fading and channel estimation problems commonly experienced in practical situations. This integrated method enables our system to concurrently attain elevated data speeds, improved bit error rate performance, and enhanced resilience against channel impairments in comparison to previous standalone or less optimized IM-DCSK methods.

The main contribution of this study is outlined below:

1) The 5G NR-LDPC code is integrated into the GJSTIM-DCSK modulation to enhance the BER performance under both multipath Rayleigh fading and AWGN channel conditions. Additionally, the 5G NR-LDPC code is also integrated with other index modulation systems based on DCSK, such as GSIM-DCSK-II [8] and GFTIM-DCSK-II [12], and their performance is evaluated against the proposed system's across both Rayleigh fading and AWGN channel environments.
2) The performance of 5G NR-LDPC-GJSTIM-DCSK is analyzed for various parameters such as codeword length, spreading factor, and code rate. Furthermore, the computational complexity of the suggested coded system is calculated and contrasted with the complexity of the uncoded GJSTIM-DCSK for various codeword lengths.

The subsequent sections of this article are organized as presented below: Section II briefly reviews the structure of the 5G NR-LDPC code. The encoding and decoding techniques employed are overviewed in Section III. The system model is outlined in Section IV. Section V then showcases and analyzes the Simulation findings. Section VI includes complexity calculations. This work concludes in Section VII.

II. NR-LDPC Code's Structure

LDPC codes fall under the category of linear-block codes, implying that a codeword $\mathbf{c} = [c_1\ c_2 \cdots c_N]$ of length N bits is derived from the K-bit information vector $\mathbf{d} = [d_1 d_2 \cdots d_K]$, this code characterized by its Parity check matrix $\mathbf{H}$ with sparse properties, that mean the number of ones in the $\mathbf{H}$ more less than ($M \times N$), with M standing for the count of parity checks, is equal to $N–K$, and the code rate R is equal to N/K.

LDPC codes are categorized as a regular and an irregular code according to whether the weight of rows and columns in the $\mathbf{H}$ matrix is consistent or inconsistent [24].

Furthermore, a Tanner graph, which defines the $\mathbf{H}$ matrix, features two types of nodes: BN (Bit nodes) represent the bits in the codeword, equaling N, the number of columns in the $\mathbf{H}$ matrix. And the check nodes (CN) represent parity checks, whose quantity is M, equivalent to the row count of the $\mathbf{H}$ matrix. In the tanner graph, the BN_j is connected to the CN_i by edge denoted by e_{ji}, if the corresponding element h_{ij} of $\mathbf{H}$ matrix is equal to one.

An example of $\mathbf{H}$ matrix for an irregular LDPC code, and its associated Tanner graph, are shown in Fig. 1.

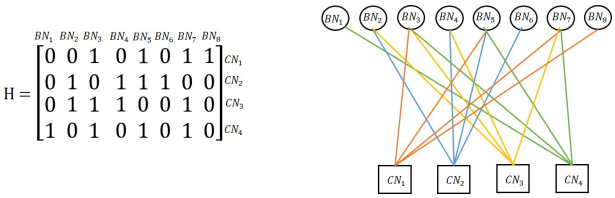

Fig. 1. Example H matrix and tanner graph for an irregular LDPC code.

In 5G NR-LDPC codes, the $\mathbf{H}$ matrix originates from the expansion of two base graphs, BG1 and BG2, using right-shift permutation matrices. In this process, each element in the base graph with shift coefficient V_{ij} is mapped to $\mathbf{I}_z^{P_{ij}}$, where $\mathbf{I}_z^{P_{ij}}$ refers to identity matrix shifted to the right by P_{ij} times with dimensions of $Z \times Z$ and Z is an expansion factor, $0 \le P_{ij} \le Z$, where $P_{ij} = \mathrm{mod}(V_{ij}, Z)$, except the case of $V_{ij} = -1$, the P_{ij} will be (-1). That mean the element with zero shift transform to identity matrix $\mathbf{I}_z$ and the elements with P_{ij} shift transform to $\mathbf{I}_z^{P_{ij}}$, while other element with -1 shift transformed to zero matrix $\mathbf{0}_{z \times z}$, all sift coefficients for BG1 and BG2 are mentioned in 3rd Generation Partnership Project [25].

For instance, BG1 is designed for transmitting long messages and operating at a higher code rate, while BG2 is utilized for short messages and a lower code rate. Their dimensions reflect these distinct purposes: BG1 has dimensions of 46×68, whereas BG2 is characterized by dimensions of 42×52. The expansion factor of 5G NR-LDPC codes can be determined as mention in [25] according to

$$Z = \partial 2^J \tag{1}$$

where J is the exponent integer, and $J \in \{0, 1, 2, \cdots, J_\partial\}$ and the value of J_∂ selects corresponding to ∂'s value as a Table I.

Table I: Selecting the Index J_∂ and Z Sets Corresponding to the Parameter ∂

∂	J_∂	J	Expansion factor $\boldsymbol{Z = \partial\, 2^J}$ sets
2	7	{0,1,2,3,4,5,6,7}	{2,4,8,16,32,64,128,256}
3	7	{0,1,2,3,4,5,6,7}	{3,6,12,24,48,96,192,384}
5	6	{0,1,2,3,4,5,6}	{5,10,20,40,80,160,320}
7	5	{0,1,2,3,4,5}	{7,14,28,56,112,224}
9	5	{0,1,2,3,4,5}	{9,18,36,72,144,288}
11	5	{0,1,2,3,4,5}	{11,22,44,88,176,352}
13	4	{0,1,2,3,4}	{13,26,52,104,208}
15	4	{0,1,2,3,4}	{15,30,60,120,240}

Therefore, several expansion factors exist based on the set of J with maximum value of Z =384. After expansion the length of the codeword becomes N=68Z for BG1 and N=52Z for BG2. Whereas K=$k_b Z$, where k_b refers to number of bits assigned to information message in BG. This value is determined by the BG number, for BG1 k_b=22 while for BG2, k_b is set to 10 if K>640, its 9 for 560<K≤640; 8 if 192<K≤560, and 6 otherwise.

Through the application of shortening and puncturing, 5G NR-LDPC codes achieve adaptability in their code rate and block length, shortening involves adding zeros to the

information bits only, whereas puncturing affects both information and parity bits within the codeword.

III. 5G NR-LDPC Encoding and Decoding Algorithm

A. Encoding Algorithm

The encoder algorithm that is used in this paper is proposed in [26]. The goal of encoding process involves calculating the parity bits from the message bits and the **H** matrix, where $\mathbf{H} \in \mathbb{B}^{M \times N}$ by solving the checksum equation.

$$\mathbf{H}\mathbf{c}^T = 0 \tag{2}$$

where **c** is the codeword sequences of length N bit and represented by $\mathbf{c} = [\mathbf{d}\mathbf{P}^T]$, $\mathbf{d} = [d_1\ d_2 \cdots d_{k_b}]$refers to the information vector of length k_b, as each element of **d** constitutes a vector with a length of Z bits, and $\mathbf{P} = [p_1\ p_2 \cdots p_M]^T$ refers to parity vector of length M bits. As presented in Fig. 2, the columns of the **H** matrix are classified into three class: information, core parities and extension parities. The rows, conversely, are categorized into core checks and extension checks. Furthermore, the **H** matrix is composed entirely of five submatrices:: **A**, **B**, **0**, **C** and **I** [23].Where $\mathbf{A} \in \mathbb{B}^{4Z \times K}$, $\mathbf{B} \in \mathbb{B}^{4Z \times 4Z}$, **0** is zero matrix with dimensions equal to $4Z \times (M-4Z)$, $\mathbf{C} = [\mathbf{C}_1, \mathbf{C}_2] \in \mathbb{B}^{(M-4Z) \times (K+4Z)}$, $\mathbf{C}_1 \in \mathbb{B}^{(M-4Z) \times K}$, $\mathbf{C}_2 \in \mathbb{B}^{(M-4Z) \times 4Z}$, and **I** is identity matrix with dimensions of $(M-4Z) \times (M-4Z)$.

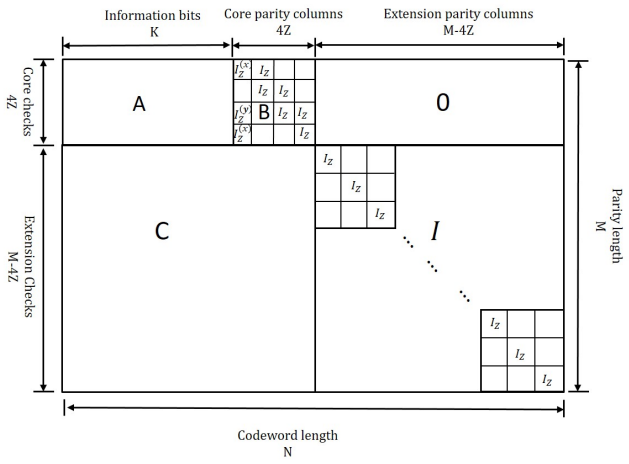

Fig. 2. Structure of the parity check matrix in NR-LDPC codes.

Furthermore, parity bits vector **P** divided into two parts: the first $4 \times Z$ which represent the core parity bits denoted as $\mathbf{p}_c = [\mathbf{p}_{c1}\ \mathbf{p}_{c2}\ \mathbf{p}_{c3}\ \mathbf{p}_{c4}]^T$, where $\mathbf{p}_c \in \mathbb{B}^{4Z \times 1}$ and each element of $\mathbf{p}_c$ has dimensional of $Z \times 1$, while the second part represents the extension parity bits denoted as $\mathbf{p}_e = [p_{e1} \cdots p_{e(M-4Z)}]^T$, where $\mathbf{p}_e \in \mathbb{B}^{(M-4Z) \times 1}$. Thus, the codeword can be represented as $\mathbf{c} = [\mathbf{d}\ \mathbf{p}_c^T\ \mathbf{p}_e^T]$, where $\mathbf{d} \in \mathbb{B}^{1 \times K}$. The encoding of LDPC codes is performed using (2), which can be expressed as

$$\begin{bmatrix} \mathbf{A} & \mathbf{B} & \mathbf{0} \\ \mathbf{C_1} & \mathbf{C_2} & \mathbf{I} \end{bmatrix} \begin{bmatrix} \mathbf{d}^T \\ \mathbf{p}_c \\ \mathbf{p}_e \end{bmatrix} = \mathbf{0} \tag{3}$$

Subsequently, (3) splits into two matrix equations as

$$\mathbf{A}\mathbf{d}^T + \mathbf{B}\mathbf{p}_c + \mathbf{0}\mathbf{p}_e = \mathbf{0} \tag{4}$$

$$\mathbf{C}_1\mathbf{d}^T + \mathbf{C}_2\mathbf{p}_c + \mathbf{I}\mathbf{p}_e = \mathbf{0} \tag{5}$$

First $4 \times Z$ core parity bits can be calculated through (4), utilizing the double diagonal sub matrix **B** and **A** sub-matrix, where

$$\mathbf{A} = [\mathbf{a}_1\ \mathbf{a}_2\ \mathbf{a}_3\ \mathbf{a}_4]^T \text{ and } \mathbf{a}_i \in \mathbb{B}^{Z \times K}$$

$$\boldsymbol{B} = \begin{bmatrix} \mathbf{I}_Z^{(x)} & \mathbf{I}_Z & \mathbf{0}_Z & \mathbf{0}_Z \\ \mathbf{0}_Z & \mathbf{I}_Z & \mathbf{I}_Z & \mathbf{0}_Z \\ \mathbf{I}_Z^{(y)} & \mathbf{0_Z} & \mathbf{I}_Z & \mathbf{I}_Z \\ \mathbf{I}_Z^{(x)} & \mathbf{0}_Z & \mathbf{0}_Z & \mathbf{I}_Z \end{bmatrix}$$

where $(.)^{(\vartheta)}$ is right circular shift by ϑ times, and ϑ represent the shift value corresponding to row and column index of the selected base graph [25]. Equation (4) can be expressed as

$$\begin{bmatrix} \mathbf{a}_1 \\ \mathbf{a}_2 \\ \mathbf{a}_3 \\ \mathbf{a}_4 \end{bmatrix} \mathbf{d}^T + \begin{bmatrix} \mathbf{I}_Z^{(x)} & \mathbf{I}_Z & \mathbf{0}_Z & \mathbf{0}_Z \\ \mathbf{0}_Z & \mathbf{I}_Z & \mathbf{I}_Z & \mathbf{0}_Z \\ \mathbf{I}_Z^{(y)} & \mathbf{0}_Z & \mathbf{I}_Z & \mathbf{I}_Z \\ \mathbf{I}_Z^{(x)} & \mathbf{0}_Z & \mathbf{0}_Z & \mathbf{I}_Z \end{bmatrix} \begin{bmatrix} \mathbf{p}_{c1} \\ \mathbf{p}_{c2} \\ \mathbf{p}_{c3} \\ \mathbf{p}_{c4} \end{bmatrix} = \mathbf{0} \tag{6}$$

Therefore, four simulated matrix equations produced from the rows of the above equation, by adding these four equations, the parity $\mathbf{p}_{c2}, \mathbf{p}_{c3}, \mathbf{p}_{c4}$ are removed, and the $\mathbf{p}_{c1}$ can be calculated as

$$\mathbf{A}\mathbf{d}^T + \mathbf{p}_{c1}^{(y)} = 0 \tag{7}$$

Since, $\mathbf{I}_Z^{(y)}\mathbf{p}_{c1} = \mathbf{p}_{c1}^{(y)}$, the first parity node can be obtained as

$$\mathbf{p}_{c1} = (\mathbf{A}\mathbf{d}^T)^{(Z-y)} \tag{8}$$

Subsequently, the remaining core parity check can be obtained through using (first, second and third) rows simulated equations from (6) and through substituting $\mathbf{p}_{c1}$ as follows:

$$\mathbf{p}_{c2} = \mathbf{a}_1\mathbf{d}^T + \mathbf{I}_Z^{(x)}\mathbf{p}_{c1} \tag{9}$$

$$\mathbf{p}_{c3} = \mathbf{a}_2\mathbf{d}^T + \mathbf{p}_{c2} \tag{10}$$

$$\mathbf{p}_{c4} = \mathbf{a}_3\mathbf{d}^T + \mathbf{I}_Z^{(y)}\mathbf{p}_{c1} + \mathbf{p}_{c3} \tag{11}$$

After that, the extension parity bits $\mathbf{p}_e$ can be easily obtained by substituting core parity bits $\mathbf{p}_c$ in (5) as

$$\mathbf{p}_e = \mathbf{C}_1\mathbf{d}^T + \mathbf{C}_2\mathbf{p}_c \tag{12}$$

By implementing this LDPC encoding technique,

matrix multiplication is replaced with a simpler process of circularly shifting corresponding bit sequences as example below:

$$\mathbf{I}_Z^{(\vartheta)}[u_0, u_1, \cdots, u_{Z-1}]^T = [u_\vartheta, u_{\vartheta+1}, \cdots, u_{Z-1}, u_0, u_1, u_{\vartheta-1}] \quad (13)$$

Also, utilizing the sparsity properties, we can ignore those $P_{ij} = -1$.

Therefore, instead work on the parity check matrix or its exponent matrix, we can directly work on the reduced shift coefficient tables [25], where the entries equal to –1 are ignored, for BG1 there are 316 circular shifts involved and for BG2 only 197 shifts.

B. Decoding Algorithm

For our system model, the layered improved offset min-sum decoding algorithm is used [27, 28], the LDPC decoder is used as SISO decoder, and the message propagated through the decoder is the LLR (log likelihood ratio) of each bit node. The initial channel LLR for each bit in the received vector $\boldsymbol{y} = [y_1\ y_2 \cdots y_j \cdots y_N]$, can be calculated as:

$$\mathrm{LLR}(j) = \log \frac{p(c_j=0/y_j)}{p(c_j=1/y_j)}, \quad (14)$$

where c_j is the *j*th bit of transmitted sequence and y_j is *j*th bit of received sequence. For AWGN channel the value of its LLR will be $\mathrm{LLR}(j) = (2/\sigma^2)y_j$, where $\sigma^2 = N_0/2$ refers to variance of received bits as Gaussian random variable. In the decoder, the message propagates iteratively between the BNs and CNs for the sparsity matrix **H**, which are defined in Section II in Fig. 1.

Moreover, this decoder employs the LLR of the complete received vector along with data from the previously decoded bit to predict the upcoming bits. A given check node CNi connects to a group of bit nodes represented by $\forall_i$, while a collection of check nodes connected to specific BNj are presented by Λ_j, these connections depend on the non-zero entries of the **H** matrix, where $h_{i,j} = 1$. Also, the message passing from BN_j to CN_i denoted as $B_{j\to i}$, where $C_{i\to j}$ refers to message passing from CN_i to BN_j.

For the 5G NR-LDPC layered decoding, each row in the BG1 or BG2 is considered a layer, which corresponds to *Z* rows in **H** matrix. Therefore, BG1 and BG2 comprise 46 and 42 layers, respectively [29]. The offset min-sum (OMS) decoding algorithm is applied to all layers in each iteration. The updated LLRs of each bit node in all CNs of the previous layer is used as input LLRs for the next layer. The channel LLRs from (14) are used to initialize the bit node LLRs for the first layer in the initial decoding iteration, as below:

$$B_j = \mathrm{LLR}(j) \quad (15)$$

and $C_{i\to j} = 0$, $B_{j\to i} = 0$ as initialization.

The following process repeated for each layer and for each BN_j subsequently:

$$B_{j\to i} = B_j - C_{i\to j,\mathrm{OMS}} \quad (16)$$

$$C_{i\to j} = \prod_{m\in\forall_i\setminus j} \mathrm{sgn}(B_{m\to i}) \times \min_{m\in\forall_i\setminus j}(|B_{m\to i}|) \quad (17)$$

The message passing from check nodes to connected bit nodes with an offset value q is described as:

$$C_{i\to j,\mathrm{OMS}} = \max\left(\left|C_{i\to j}\right| - q, 0\right) \quad (18)$$

where $0 < q < 1$, In this paper, the value of q is selected to be 0.5.

$$B_j = B_{j\to i} + C_{i\to j,\mathrm{OMS}} \quad (19)$$

where $C_{i\to j,\mathrm{OSM}}$ is the last update calculated from (18), while (17) utilizes the value of $C_{i\to j,\mathrm{OMS}}$ that was stored at the beginning of the layer.

The B_j represents the updated LLR of each bit node in the concerned layer, which is used later as input LLR for the next layer. The hard decision is made using the output LLR of each iteration as:

$$\widehat{c_j} = \begin{cases} 0, & \text{for } B_j \geq 0 \\ 1, & \text{for } B_j < 0 \end{cases} \quad (20)$$

Typically, the algorithm is executed until either the maximum iteration count is reached, or the parity check defined in (2) is satisfied through the previously noted hard decision. The layered OSM decoder converges faster, uses fewer iterations, and achieves better error performance.

IV. 5G NR-LDPC-GJSTIM-DCSK Scheme

A. The Transmitter Structure

Fig. 3 illustrates the proposed system's transmitter model. As an initial stage, the *A* bits of the message represented by vector **a** are encoded into *N* bits of codeword **c** using encoder algorithm mentioned in Section III.

Before the message enters the encoder, it is concatenated with zero bits, called filler bits, of length n_f, since $A = K\text{-}n_f$. In order to make its length compatible with *K* information bits in 5G NR-LDPC code where $K = 22Z$ or $K = 10Z$ for BG1 and BG2, respectively.

Subsequently, the codeword **c** inputs to the rate-matching function in which shortening and puncturing methods are utilized to achieve greater adaptability in code rate and block length, here the length of the codeword **c** changes from *N* to *E* after the rate-matching and codeword **e** is produced. Thus the 5G NR-LDPC codes are represented by (*E*, *A*) codes, where *R*= *A* /*E* refers to the code rate, whereas *A* and *E* refer to information message length and transmitted codeword length, respectively.

Then, the *E* bits of the codeword **e** are divided into ψ frame, where $\mathbf{e} = [\mathbf{e}_1, \mathbf{e}_2, \cdots, \mathbf{e}_n, \cdots, \mathbf{e}_\psi]$, $n = 1,2,\cdots,\psi$ and $\mathbf{e}_n$ refers to *n*th frame. All ψ frame are sequentially modulated by the GJSTIM-DCSK system.

Each frame consists of P_T bit, so $\mathbf{e}_n =$

$[e_{n,1}, e_{n,2}, \cdots, e_{n,P_T}]$, where $P_T = Gp$ refers to the total number of bits transmitted via one GJSTIM-DCSK system symbol. After that, each frame of length P_T is split into G groups, the p bit transmit through each group are calculated as:

$$p = p_s + (N_s - N_{\text{as}})p_t + N_{\text{as}}N_t + (N_s - N_{\text{as}})(N_t - N_{\text{st}}) \quad (21)$$

here $p_s = \left\lfloor \log_2 \binom{N_s}{N_{\text{as}}} \right\rfloor$ bits refer to the number of the subcarrier mapping bits. These bits are used to select the N_{as} active subcarriers indices out of N_s subcarriers through combinatorial mapping in each group, Additionally, $p_t = \left\lfloor \log_2 \binom{N_t}{N_{\text{st}}} \right\rfloor$ bits refer to the count of the time mapping bits. These bits are used to select N_{st} time slots indices out of N_t for $(N_s - N_{\text{as}})$ idle subcarriers [14], where N_s and N_t refer to the count of subcarrier in one group and the count of time slot, respectively.

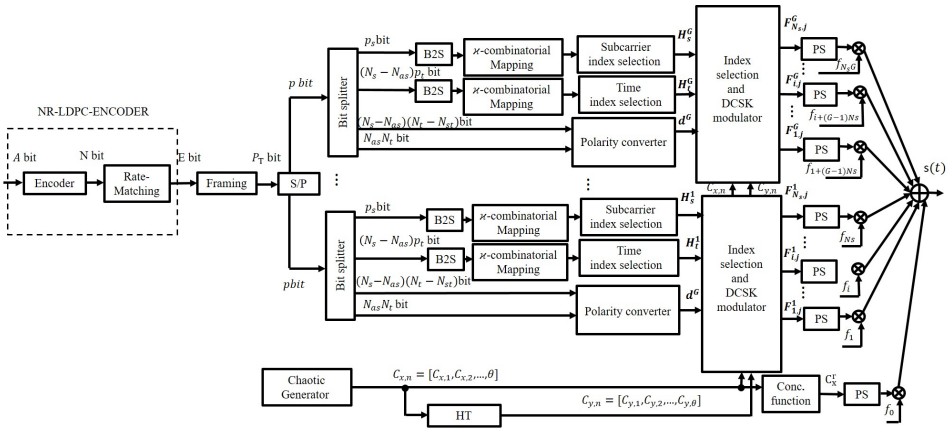

Fig. 3. NR-LDPC-GJSTIM-DCSK's transmitter structure.

The function $\binom{\cdot}{\cdot}$ refers to a combinatorial coefficient, which is used to calculate the number of possible combinations, and $\lfloor \cdot \rfloor$ refers to the floor function. In addition to mapping bits, the p bits contain the DCSK-modulated bits, which comprise $N_{\text{as}}N_t + (N_s - N_{\text{as}})(N_t - N_{\text{st}})$.

The initial $N_{as}N_t$ bits are conveyed through every time slot of active subcarriers, while the remaining $(N_s - N_{\text{as}})(N_t - N_{\text{st}})$ bits are transmitted through non-selected time slots in the idle subcarriers, where N_s and N_{as} refer to the total sub-carriers number and the active sub-carriers number in each group, respectively, while N_t and N_{st} denote the total count of time slots and the count of selected time slots, respectively, in each group of the GJSTIM-DCSK system.

The chaotic sequence $C_{x,n}$ with length of θ is produced using a second order-Chebyshev polynomial function, meanwhile, the Hilbert transform (HT) function is employed to derive an orthogonal chaotic sequence $C_{y,n}$ from the reference chaotic sequence $C_{x,n}$ [14].

The GJSTIM-DCSK system contains $2^\rho + 1$ sub-carriers; One is allocated for carrying reference vector $C_{x,n}$ and the other 2^ρ subcarriers are then divided into $G = 2^\rho / N_s$ groups, with each group consisting of N_s sub-carriers, where ρ is an integer and $(\rho \geq p_s)$.

Subsequently, for every group of the frame, the p_s bits are transformed into a symbol. Then, combinatorial mapping is used to convert this symbol into a vector of active sub-carrier indices with N_{as} length, which is represented by $\mathbf{H}_{\text{s}}$. In the same way, mapping is applied to the p_t bits to identify the chosen time slot indices of $(N_s - N_{\text{as}})$ idle subcarriers, where $\mathbf{H}_t$ is the matrix of the selected time slot indices with $(N_s - N_{\text{as}}) \times N_{\text{st}}$ dimensions.

The complement is taken for each row vector $\mathbf{h}_t$ of $\mathbf{H}_t$ matrix to obtain the unselected time slot indices vector of each idle subcarrier. These indices are represented by $\widetilde{\boldsymbol{h}_t}$ of $(N_t - N_{\text{st}})$length.

Afterwards, the $N_{as}N_t$ bits are modulated by $C_{x,n}$ and are carried by all time slots of the activesub-carriers, while $(N_s - N_{\text{as}})(N_t - N_{\text{st}})$ bits are modulated by $C_{y,n}$ and are carried by unselected time slots of idle sub carriers.

After the index-selection and DCSK-modulation of each group, the output of these blocks is represented by

$$F_{i,j}^g = \begin{cases} d_{i,j}^g C_{x,n}, & \text{for } i \in \mathbf{H}_s^g, j = 1,2,\cdots,N_t \\ 0, & i \notin \mathbf{H}_s^g, j \in \mathbf{H}_t^g \\ d_{i,j}^g C_{y,n}, & \text{for } i \notin \mathbf{H}_s^g, j \in \widetilde{\mathbf{H}_t^g} \end{cases} \quad (22)$$

Here g refers to the group index and $d_{i,j}$ refers to the modulated bits after polarity converter carried by ith sub-carriers and jth time slot, where $d_{i,j} \in \{1, -1\}$. After that, the reference signal $C_{x,n}$ is repeated N_t times making its length extended to β, here β represents the system's spreading factor and equals to $(N_t\theta)$. Lastly, the data-carrying signal $\mathbf{F}^g$ and repeated reference $\mathbf{C}_x^r$ inter pulse-shaping filters to produce the analogy version of these signals as $F^g(t)$ and $C_x^r(t)$.

The transmitted signal of 5G NR-LDPC-GJSTIM-DCSK for each frame can be expressed as:

$$s(t) = C_x^r(t)\cos(2\pi f_0 t + \phi_0) + \sum_{g=1}^{G}\sum_{i=1}^{N_s}\sum_{j=1}^{N_t} F_{i,j}^g(t)\cos\left(2\pi f_{(g-1)N_s+i}t + \phi_{(g-1)N_s+i}\right) \quad (23)$$

The frequencies utilized in the proposed system are orthogonal. Here f_0 and ϕ_0 refer to the subcarrier's center frequency and phase angle of that is used to carry the repeated chaotic signal. Meanwhile $f_{(g-1)N_s+i}$ and $\phi_{(g-1)N_s+i}$ refer to the center frequencies and the phase angle of ith subcarrier and gth group.

The algorithm of 5G NR-LDPC-GJSTIM-DCSK's transmitter is presented in Algorithm 1. First, the information and the necessary parameters used in the proposed system are identified, including ($\mathbf{a}$, N_s, N_{as}, N_t, N_{st}, P_T, p, p_t, p_s, k_{mappin}, $\mathbf{C}_x$, $\mathbf{C}_y$, θ and LDPC-info). Here LDPC-info refers to all information related to LDPC code that is produced based on E and A such as the values of (Z, N, K number of BG, and n_f).

Algorithm 1: 5G NR-LDPC-GJSTIM-DCSK Transmitter.

Input: (information , $E, R, A, \mathbf{a}$, LDPC − info)
LDPC- message=[$\mathbf{a}$, zeros (1, n_f)]
$\mathbf{c}$ = NR-LDPC-Encoder (LDPC-info, LDPC- message)
$\mathbf{e}$ =NR-LDPC-Rate-Matching (LDPC-info, $\mathbf{c}$, E)
$\psi = \lfloor E/P_T \rfloor + 1$, $G = \lfloor \psi/p \rfloor$, $\mathbf{s}_T = [\,]$
For i=1,.., ψ do
  For $g = 1,2, \dots, G$ do
    $\mathbf{s}_T^g$ =GJSTIM-DCSK-Modulation($\mathbf{e}_{i,g}$)
    $\mathbf{s}_T = [\mathbf{s}_T \ \mathbf{s}_T^g]$
  End
End
Output : $\mathbf{s}_T$ total transmitted signal.

In Step 1, the LDPC- message is generated from the message vector $\mathbf{a}$ by adding a zero column vector of length n_f. In step 2, the codeword $\mathbf{c}$ of length N is produced using 5G NR-LDPC-Encoder. The rate matching function is applied to the codeword $\mathbf{c}$ to produce the vector $\mathbf{e}$ of length E, as depicted in step 3. After that, vector $\mathbf{e}$ is framed into ψ frames, each with length P_T bits, where $\psi = \lfloor E/P_T \rfloor + 1$. Then, each of the ψ frames is divided into G group to produce $\mathbf{e}_{i,g}$ vector of the ith frame and gth group with length p. In step 7, the GJSTIM-DCSK-Modulation function is applied to each $\mathbf{e}_{i,g}$ to produce the transmitted signal of every group $\mathbf{s}_T^g$ and subsequently the total transmitted signal $\mathbf{s}_T$.

B. The Receiver Structure

multipath Rayleigh fading channel affects the transmitted signal, which is also corrupted by an AWGN signal $\mu(t)$ of zero mean and $n_0/2$ variance, the received signal is then

$$r(t) = \sum_{l=1}^{\mathcal{L}} \alpha_l s(t-\tau_l) + \mu(t) \tag{24}$$

Here, α_l and τ_l represent the channel coefficient and time delay of the lth path, respectively, and $\mathcal{L}$ refers to the paths number. It is generally considered that the coefficients α_l are Rayleigh random variables. There are at least two pathways in the Rayleigh fading scenario, in contrast, the AWGN situation involves merely a single path and a single channel coefficient. Fig. 4 illustrates the receiver structure of the proposed system, just frame period is taken into consideration for the purpose of simplicity. Initially, separation of the received signals is achieved using $2^\rho + 1$ orthogonal modulated carrier frequencies. Subsequently, the matching filters acquire samples of these signals at nT_c. In discrete outputs, the recurrent chaotic signal is recorded in matrix $\mathbf{W} \in \mathbb{B}^{1\times\beta}$ and the information-bearing signal in matrix $\mathbf{S}^g \in \mathbb{B}^{N_s\times\beta}$ for the g th group. The reference signal matrix is expressed as:

$$\mathbf{W} = [\mathbf{W}_1, \cdots, \ \mathbf{W}_j, \cdots, \ \mathbf{W}_{N_t}] \tag{25}$$

and the matrix $\mathbf{S}^g$ can be described as:

$$\mathbf{S}^g = \begin{bmatrix} \mathbf{S}_{1,1}^g & \cdots & \mathbf{S}_{1,N_t}^g \\ \vdots & \ddots & \vdots \\ \mathbf{S}_{N_s,1}^g & \cdots & \mathbf{S}_{N_s,N_t}^g \end{bmatrix} \tag{26}$$

where $\mathbf{W}_j = [w_j(1), w_j(2), \cdots, w_j(\theta)]$, $j = 1,2,\cdots,N_t$, and $\mathbf{S}_{i,j}^g = \left[s_{i,j}^g(1), s_{i,j}^g(2), \cdots, s_{i,j}^g(\theta)\right]$, $i = 1,2,\cdots,N_s$, $j = 1,2,\cdots,N_t$, $g \in \{1,2,\cdots,G\}$ [14]. Vector $\boldsymbol{W}$ is then filtered using the averaging filter over a N_t window. This approach involves summing and averaging data across N_t segments of θ-length chaotic sequences based on their location.

The output is expressed as [14]:

$$\boldsymbol{R}_x = \frac{1}{N_t}\sum_{j=1}^{N_t} \mathbf{W}_j = \sum_{l=1}^{L} \alpha_l \, \mathbf{C}_{x,\tau_l} + \widetilde{\boldsymbol{\mu}_R} \tag{27}$$

where ($\widetilde{\boldsymbol{\mu}_R}$) denotes AWGN, which corresponds to the averaged chaotic reference ($\boldsymbol{R}_x$), having a variance of $N_0/2N_t$ and a zero mean. An orthogonal vector to $\boldsymbol{R}_x$, represented as $\mathbf{R}_y$, is then created by applying a Hilbert transform to $\mathbf{R}_x$. Subsequently, the $\mathbf{D}_s^g$ correlator matrix is calculated using the correlated averaged reference $\mathbf{R}_x$ with $\mathbf{S}^g$ in order to identify the active subcarrier indices $\mathfrak{U}_s^g$ in the gth group, where $\mathbf{D}_s^g \in \mathbb{R}^{N_s\times N_t}$.

$$\mathbf{D}_s^g = \begin{bmatrix} \mathbf{R}_x(\mathbf{S}_{1,1}^g)^T & \cdots & \mathbf{R}_x(\mathbf{S}_{1,N_t}^g)^T \\ \vdots & \ddots & \vdots \\ \mathbf{R}_x(\mathbf{S}_{N_s,1}^g)^T & \cdots & \mathbf{R}_x(\boldsymbol{S}_{N_s,N_t}^g)^T \end{bmatrix} \tag{28}$$

Algorithm 2 delineates the process for detecting the indices of active subcarriers. This algorithm requires the correlator matrix ($\mathbf{D}_s^g$) and the parameters N_s, N_{as}, k-mapping, and p_s as inputs.

Algorithm 2: Active subcarrier index detection and mapping subcarriers index bits to soft symbol for the gth group

Input:N_s,N_{as},$\mathbf{D}_s^g$, k-mapping, p_s
For $i = 1,2,\cdots,N_s$ do
  $\boldsymbol{D}_{\max}(i) = \max\left(\left|\mathbf{D}_S^g(i,:)\right|\right)$
End
For j = $1,2,\cdots,\mathrm{N_{as}}$ do
  [~,r_s]=find{|$\mathbf{D}_{\max}$|=max(|$\mathbf{D}_{\max}$|)}
  $D(r_s)$=0; $\mathfrak{U}_s^g$(j) = r_s
End
$\mathfrak{U}_s^g = sort(\mathfrak{U}_s^g)$; $\widetilde{\mathfrak{U}_s^g}$=complement($\mathfrak{U}_s^g$)
For $l = 1,2,\dots,2^{p_s}$ do
  If $\mathfrak{U}_s^g$=k-mapping (l ,:) then
    $x_c{}^g = l$

End
End
$x_c{}^g = x_c{}^g - 1$
$\mathbf{m}^g$ =decimal to bit (x_c,p_s)
$\mathbf{c}_s{}^g = 2\mathbf{m}^g - 1$
Output: $\mathfrak{U}_s^g$, $\widetilde{\mathfrak{U}_s^g}$, $\mathbf{m}^g$, $\mathbf{c}_s{}^g$

From the N_s variables, the algorithm determines the N_{as} largest values and subsequently records these values in the vector $\mathfrak{U}_s^g$, which represents the index vector of active subcarrers. Afterwards, $\mathfrak{U}_s^g$ is organized in a manner that yields the vector corresponding to its own arrangement. The complement of $\mathfrak{U}_s^g$ is computed to obtain the indices of the idle subcarriers, allowing for the retrieval of the remaining bits within them. This is accomplished by By taking the complement of the elements in $\mathfrak{U}_s^g$ within the group $\{1, 2, \cdots, N_s\}$.The vector $\mathfrak{U}_s^g$ is transformed into the symbol $x_c{}^g$ through k-mapping, and this symbol is converted into binary in order to identify the active subcarrier index bits denoted as $\mathbf{m}^g = [m_1, m_2, \cdots, m_{p_s}]$. Then, these bits are converted into bipolar form as $\mathbf{c_s}{}^g = 2\mathbf{m}^g - 1$.

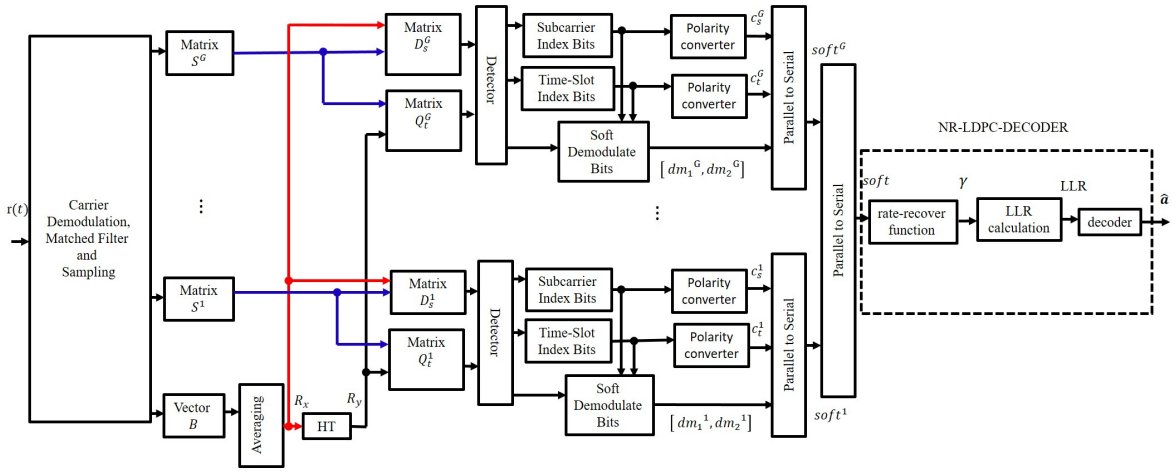

Fig. 4. 5G NR-LDPC-GJSTIM-DCSK's receiver structure.

Upon identifying the active subcarriers, the soft demodulated data can be determined by the real decision variable within the rows corresponding to the active subcarriers in the matrix $\mathbf{D}_s^g$. This can be denoted by a vector $\mathbf{dm}_1^g$ of length $N_s N_t$.

For gth group, a correlator matrix $\mathbf{Q}_t^g$ of dimension (N_s–N_{as})×N_t is constructed to facilitate the recovery of message bits transmitted by the idle subcarriers.

This is accomplished by performing a correlation between the orthogonal reference denoted as $\mathbf{R}_y$, with (N_s–N_{as}) rows of $\mathbf{S}^g$. These rows correspond to the indices of idle subcarriers within the vector $\widetilde{\mathfrak{U}_s^g}$ with a length of (N_s–N_{as}).

$$\mathbf{Q}_t^g = \begin{bmatrix} \mathbf{R}_y(\mathbf{S}^g_{\widetilde{\mathfrak{U}_s^g}(1),1})^T & \cdots & \mathbf{R}_y(\mathbf{S}^g_{\widetilde{\mathfrak{U}_s^g}(1),N_t})^T \\ \vdots & \ddots & \vdots \\ \mathbf{R}_y(\mathbf{S}^g_{\widetilde{\mathfrak{U}_s^g}(N_s-N_{\text{as}}),1})^T & \cdots & \mathbf{R}_y(\mathbf{S}^g_{\widetilde{\mathfrak{U}_s^g}(N_s-N_{\text{as}}),N_t})^T \end{bmatrix} \quad (29)$$

Algorithm 3 executes the detection of selected time slots utilizing the matrix $\mathbf{Q}_t^g$ along with $\widetilde{\mathfrak{U}_s^g}$, N_s, N_{as}, N_t, N_{st}, k-mapping, and p_t as inputs, form N_t variables within every row of the $\boldsymbol{Q}_t^g$ matrix, the algorithm identifies the (N_t–N_{st}) largest values. These values are then recorded in the $\widetilde{\mathfrak{U}_{\text{tt}}^g}$ matrix of dimension (N_s–N_{as})×(N_t–N_{st}), which comprises unselected time slots indices within idle subcarriers.

Algorithm 3: Detection of selected time slots and soft symbol mapping for time slot index bits for the gth group

Input:N_s,N_{as}, N_t, N_{st}, $\mathbf{Q}_t^g$,p_t , k_mappin
For $i = 1, 2, \cdots, N_s - N_{\text{as}}$ do
  $\mathbf{K}_m$=$\mathbf{Q}_t^g$
  For j =1,2,⋯,$N_t - N_{\text{st}}$ do
    [~,r_s]= find{|$\mathbf{K}_{m,\max}$|==max(|$\mathbf{K}_m(i,:)$|)}
    $\mathbf{K}_m(i, r_s) = 0$; $\widetilde{\mathfrak{U}_t^g(j)} = r_s$
  End
  $\widetilde{\mathfrak{U}_t^g} = sort(\widetilde{\mathfrak{U}_t^g})$;
  $\widetilde{\mathfrak{U}_{\text{tt}}^g}(i,:) = \widetilde{\mathfrak{U}_t^g}$
  $\mathfrak{U}_t^g$ =complement ($\widetilde{\mathfrak{U}_t^g}$)
  $\mathfrak{U}_{\text{tt}}^g(i,:)$ =$\mathfrak{U}_t^g$
  For l = 1,2, ⋯, 2^{p_t}do
    If $\mathfrak{U}_{\text{tt}}^g(i,:) == k\_\text{mappin}(l,:)$
      $\mathbf{x}_t(i,:) = l$
      $\mathbf{x}_t(i,:) = \mathbf{x}_t(i,:) - 1$
    End
  End
  $\mathbf{T}^g(i,:)$ =decimal to bit ($\mathbf{x}_t(i,:)$,p_t)
  $\mathbf{c}_t^g(i,:) = 2\mathbf{T}^g(i,:) - 1$
End
$\mathbf{c}_t^g = \text{reshap}(\mathbf{c}_t^g, 1, (N_s - N_{\text{as}}) \times p_t)$
Output: $\mathfrak{U}_{\text{tt}}^g$, $\widetilde{\mathfrak{U}_{\text{tt}}^g}$, T^g,$\mathbf{c}_t^g$

Subsequently, the matrix $\mathfrak{U}_{\text{tt}}^g$ is identified as the complement of the matrix $\widetilde{\mathfrak{U}_{\text{tt}}^g}$, which comprises the indices of selected time slots. every row in $\mathfrak{U}_{\text{tt}}^g$ is subsequently mapped to the symbol x_t by performing the inverse k-mapping operation. Then, these symbols are converted into $\mathbf{T}^g$ matrix with dimensions $(N_s - N_{\text{as}}) \times p_t$ bits, representing the time slot index bits in the g^{th} group. Afterward, each bit in $\mathbf{T}^g$ matrix is transformed to soft symbol through bipolar transformation applied to each row of $\mathbf{T}^g$, the same algorithm is applied to each group.

Then, the soft demodulated data bits transmitted by idle subcarriers and unselected time slots are identified by decision variables in each row of $\boldsymbol{Q}_t^g$, specifically in columns corresponding to the non-selected time slots indices in $\widetilde{\mathfrak{U}}_{\mathrm{tt}}^g$. These decision variables are denoted as $\mathbf{dm}_2{}^g$ of length $(N_s–N_{\mathrm{as}})\times(N_t–N_{\mathrm{st}})$. Therefore, the soft output of demodulation for gth group can be represented by the vector ($\mathbf{soft}^g$) of length p as:

$$\mathbf{soft}^g = \left[\mathbf{c}_s{}^g, \mathbf{c}_t^g, \mathbf{dm}_1{}^g, \mathbf{dm}_2{}^g\right] \tag{30}$$

whereas, the soft output of the ith frame can be determined by concatenating the soft outputs of all the system's groups into a single vector of length P_T as follows:

$$\mathbf{soft}_i = \left[\mathbf{soft}_i^1, \mathbf{soft}_i^2, \cdots, \mathbf{soft}_i^g, \cdots, \mathbf{soft}_i^G\right] \tag{31}$$

where $g \in \{1,2,\cdots,G\}$, $i \in \{1,2,\cdots,\psi\}$ and G refers to the number of groups. After demodulating all received frames, which were produced by framing the E bit as the output of rate-matching at the transmitter, the soft outputs of these frames are concatenated to produce vector $\mathbf{soft}$ of length E bit.

$$\mathbf{soft} = \left[\mathbf{soft}_1, \mathbf{soft}_2, \cdots, \mathbf{soft}_i, \cdots, \mathbf{soft}_\psi\right] \tag{32}$$

Thereafter, the rate-recover function is used to retrieve the N-length of the codeword $\mathbf{c}$, from the vector $\mathbf{soft}$ of length E soft symbol. Consequently, a vector of length N soft symbol, represented as:

$$\boldsymbol{\gamma} = \left[\gamma_1, \gamma_1, \cdots, \gamma_j, \cdots, \gamma_N\right] \tag{33}$$

Then, the LLR vector can be obtained using the following formula:

$$\mathbf{LLR} = -\left[\gamma_1, \gamma_1, \cdots, \gamma_j, \cdots, \gamma_N\right] \tag{34}$$

Subsequently, the soft **LLR** proceed to the 5G NR-LDPC decoder. During the decoding process to produce estimated message bits $\hat{\mathbf{a}}$. The Algorithm 4 presents the overall processes of the receiver, where demo-info refers to all information required for GJSTIM-DCSK demodulation as (N_s, N_{as}, N_t, N_{st}, $\mathbf{Q}_{\mathrm{t}}^g$, p_t, k_mappin, $p_s, \mathbf{D}_s^g, \mathbf{R}_x, \mathbf{R}_y$), I_m refers to the maximum iteration count for the decoding operation, and LDPC − info is the same as that used in the Algorithm 2 .

Algorithm 4: suggested 5G NR-LDPC-GJSTIM-DCSK receiver algorithm

Input: (demo − info , I_m, LDPC − info)
soft = [ ],
For $i = 1,2,\cdots,\psi$ do
  $\mathbf{soft}_i$ = [ ]
  For $g = 1,2,\ldots,G$ do
    $\mathbf{soft}^g$ =GJSTIMDCSK- demodulation(demo-info)
    $\mathbf{soft}_i = [\mathbf{soft}_i \quad \mathbf{soft}^g]$
  End
  $\mathbf{soft} = [\mathbf{soft} \quad \mathbf{soft}_i]$
End
$\boldsymbol{\gamma}$ = rate-recover (LDPC-info, **soft**
LLR= $-\boldsymbol{\gamma}$
$\hat{\mathbf{a}}$ = 5G NR-LDPC-decoding(LDPC-info,I_m)
Output : $\hat{\mathbf{a}}$

V. Results and Discussion of the Simulation

To demonstrate the effectiveness of 5G NR-LDPC codes in enhancing BER performance of the GJSTIM-DCSK system across AWGN and multipath Rayleigh channels, several simulation results are provided in this section. A three-path model is used for the multipath channel, featuring an equal power profile ($E(\alpha_1{}^2) = E(\alpha_2{}^2) = E(\alpha_3{}^2) = 1/3$) and relative delays of ($\tau_1 = 0, \tau_2 = 1, \tau_3 = 2$).whereas the GJSTIM-DCSK system parameters including (G=4, $N_s = 8, N_{\mathrm{as}} = 4, N_t = 8, N_{\mathrm{st}} = 4$) are maintained constant across all simulation runs. The maximum number of iteration utilized in the decoding operation is set as $I_m = 10$.

The BER results were obtained through computer simulations performed in MATLAB (R2022b). For each simulated signal-to-noise ratio (SNR) point, 10,000 independent simulation trials were conducted to ensure the statistical reliability of the BER estimates.

Fig. 5 illustrates the proposed 5G NR-LDPC-GJSTIM-DCSK system performance in terms of BER with different codeword lengths for rate 1/3 under an AWGN channel. The 5G NR-LDPC-GJSTIM-DCSK system demonstrates better performance with increasing codeword length. For instance, the BER performance at 10^{-3} with codeword lengths of 3000, 5000, and 7648 achieves coding gains of 8.85dB, 9.05dB, and 9.35dB, respectively. The rate 1/3 performance with a codeword length of 7648 is superior to codeword lengths of 3000 and 5000, obtaining gains of 0.5 dB and 0.3dB, respectively at BER of 10^{-3}

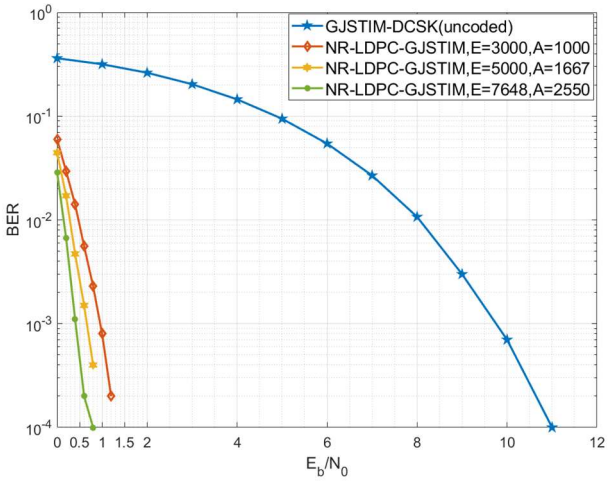

Fig. 5. 5G NR-LDPC-GJSTIM-DCSK BER performance versus E_b/N_0 for R =1/3 with different codeword lengths of E=3000, 5000, and 7648 under an AWGN.

Subsequently, the suggested system's performance was evaluated for varying code rates and spreading factors as illustrated in Fig. 6, where the codeword length is set as E=7648. As revealed in Fig. 6, rising spreading factor values result in a deterioration of BER performance, attributable to the chaotic signal accumulating more noise

as its length increases when transmitted alongside information over the channel with a non-coherent receiver.

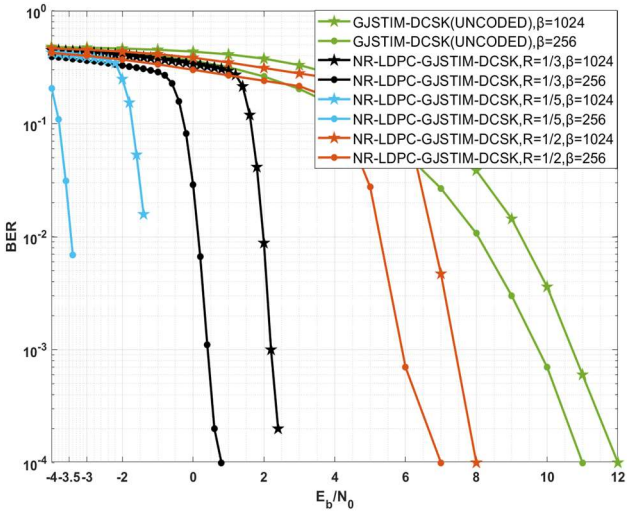

Fig. 6. 5G NR-LDPC-GJSTIM-DCSK BER performance versus E_b/N_0 for different code rates with different spreading factors, E=7648 under an AWGN.

However, a code rate of 1/5 demonstrated the best performance compared to the rates of 1/3 and 1/2. Specifically, at a BER of 10^{-1}, a code rate of 1/5 with $\beta = 256$ can obtain roughly 2.05dB gain relative to the same rate when $\beta = 1024$. Similarly, at BER of 10^{-3}, rates of 1/3 and 1/2 with $\beta = 256$ achieved gains of approximately 1.8 and 2dB, respectively, compared to the same rates when $\beta = 1024$. Furthermore, Fig. 6 illustrates that a rate of 1/5 with $\beta = 256$ achieved gains of nearly 3.6dB and 8.8dB contrasted to rates of 1/3 and 1/2, respectively, with the same β at BER=10^{-2}.

In addition, the rates of 1/5, 1/3, and 1/2 with $\beta = 256$ can achieve coding gain of about 11.6dB, 9.35dB and 3.85dB respectively, at BER=10^{-2} for rate 1/5 and BER= 10^{-3} for the 1/3 and 1/2 rates.

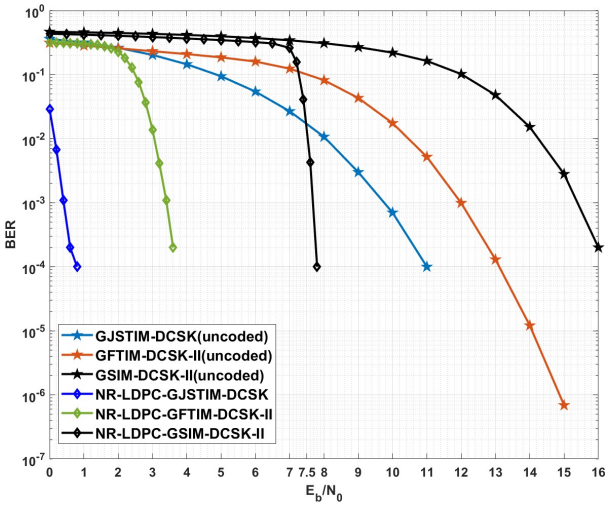

Fig. 7. 5G NR-LDPC-GJSTIM-DCSK BER performance versus other systems with R=1/3, E=7648 and β=256 under an AWGN.

Afterwards, the identical 5G NR-LDPC code was employed with alternative index modulation-based DCSK systems, including GSIM-DCSK-II [8] and GFTIM-DCSK-II [12]. The performance of these systems was then compared with the proposed system under AWGN, as depicted in Fig. 7. The NR-LDPC parameters of all systems are set to E=7648 and R=1/3. Meanwhile the modulation parameters of the alternative systems are set to $N_s = 8$, $N_t = 8$ and G=4, and $\beta = 256$ for all systems. As depicted in Fig. 7, the proposed system demonstrates superior performance compared to these other systems. It achieves an approximate gain of 3 dB and 7.12 dB relative to the 5G NR-LDPC-GFTIM-DCSK-II and 5G NR-LDPC-GSIM-DCSK-II systems, respectively, whene the BER is 10^{-3}.

In addition, the 5G NR-LDPC-GFTIM-DCSK-II and 5G NR-LDPC-GSIM-DCSK-II can achieve coding gain of about 8.6dB and 8.28dB, respectively, for BER =10^{-3}, while the suggested system can achieve a coded gain about 9.35dB.

B. The BER performance under Multipath Rayleigh Fading Channel

The 5G NR-LDPC-GJSTIM-DCSK BER performance with varying codeword lengths E=3000, 5000, 7648 for R=1/3 and β of 256 across a Rayleigh fading channel has been analyzed and compared to the performance of uncoded GJSTIM-DCSK as shown in Fig. 8. Similarly, and consistent with observations in the AWGN channel, the suggested system exhibits a notable performance improvement with increased codeword length. Specifically, a codeword length of 7648 demonstrates superior performance relative to other codeword lengths. Specifically, it achieves gains of approximately 2 dB and 1 dB compared to codeword lengths of 3000 and 500, respectively, at a BER of 10^{-3}.Whereas, in comparison with the performance of the uncoded system, the codeword lengths of 7648, 5000, and 3000 can achieve coding gains of 17 dB , 16 dB, and 14 dB, respectively, at a BER of 10^{-3}.

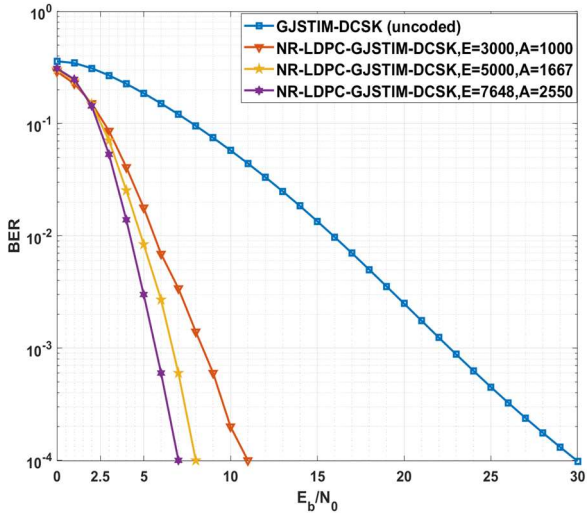

Fig. 8. 5G NR-LDPC-GJSTIM-DCSK BER performance versus E_b/N_0 for R=1/3 with different codeword lengths, E=3000, 5000, 7648 under Rayleigh fading channel.

Subsequently, the proposed system's performance has been explored with different coding rates and different spreading factors for a codeword length of 7648 over a Rayleigh fading channel, as illustrated in Fig. 9. The

performance of the system degrades with increasing spreading factor. Specifically, the system's performance across all rates is superior when $\beta = 256$ compared to when $\beta = 1024$. For instance, code rates of 1/5 and 1/3, when $\beta = 256$, achieve gains of approximately 2.3dB and 2.6dB, respectively, in contrast to when $\beta = 1024$, at a BER of 10^{-3}. Also, as shown in Fig. 9 a code rate of 1/5 demonstrates superior performance compared to a code rate of 1/3 with different β values, since it achieves coding gains of 22.2 dB and 21.2 dB compared to the performance of an uncoded system when β is 256 and 1024, respectively. Meanwhile, a code rate of 1/3 achieves coding gains of 17 dB and 15.7 dB when β is 256 and 1024, respectively, at BER of 10^{-3}.

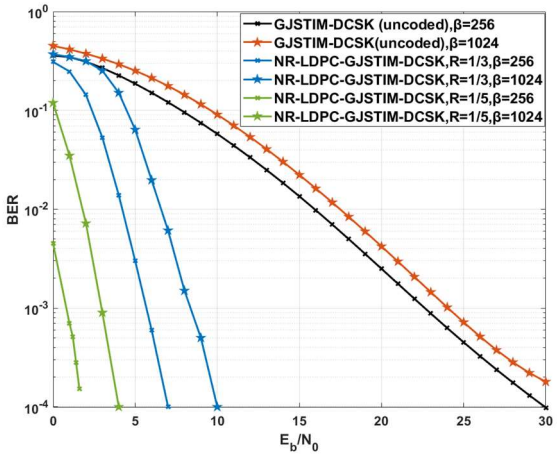

Fig. 9. 5G NR-LDPC-GJSTIM-DCSK BER performance systems versus E_b/N_0 for different code rates with different spreading factors, E=7648 under Rayleigh fading channel.

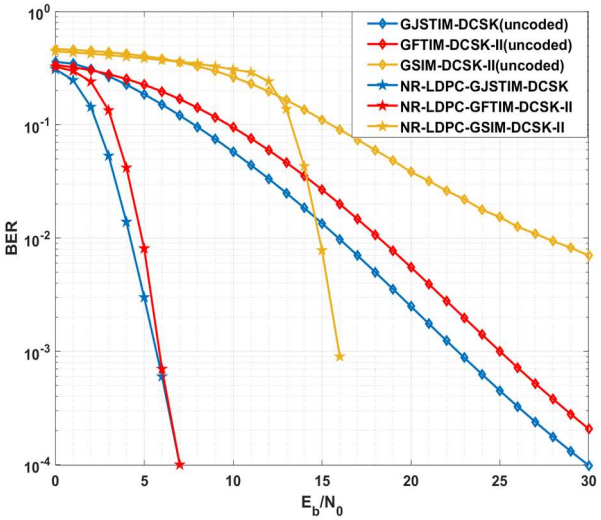

Fig. 10. 5G NR-LDPC-GJSTIM-DCSK performance versus other systems with R=1/3, E=7648, and $\beta = 256$ under Rayleigh fading channel.

Following this, the proposed system performance was evaluated relative to other systems under Rayleigh fading channel conditions. The specified systems are the same those referenced in the AWGN section, utilizing a codeword length of 7648, a spreading factor of 256, and a code rate of 1/3. As demonstrated in Fig. 10, the proposed 5G NR-LDPC-GJSTIM-DCSK performance outperforms the 5G NR-LDPC-GFTIM-DCSK-II performance at low SNRs and has an identical BER at an SNR of 7dB. Meanwhile, it outperforms the 5G NR-LDPC-GSIM-DCSK-II performance, achieving a gain of 10 dB compared to the performance of the 5G NR-LDPC-GSIM-DCSK-II at a BER of 10^{-3}.

The 5G NR-LDPC-GJSTIM-DCSK and 5G NR-LDPC-GFTIM-DCSK-II systems achieve approximately coding gains of 17 dB and 19 dB, respectively, in contrast to the performance of an uncoded scenario of these systems at BER= 10^{-3}. Whereas, the 5G NR-LDPC-GSIM-DCSK-II system attains a coded gain of 12.6 dB when the BER is10^{-2}.

VI. Complexity Analysis

The total computational complexity of the proposed 5G NR-LDPC-GJSTIM-DCSK system is derived by considering the combined complexity of the GJSTIM-DCSK system and the integrated LDPC decoder. As detailed in our previous work [14], the complexity of the GJSTIM-DCSK system, encompassing both multiplication and search operations at the transmitter and receiver, is denoted by (35).

$$O_{\text{GJSTIM}} = G\{N_{\text{as}}N_t\theta + (N_t - N_{\text{st}})(N_s - N_{\text{as}})\theta + N_sN_t\theta + (N_s - N_{\text{as}})N_t\theta + \binom{N_s}{N_{\text{as}}} + (N_s - N_{\text{as}})\binom{N_t}{N_t - N_{\text{st}}}\} \quad (35)$$

The complexity of the integrated LDPC decoder depends on the complexity of the layered OMS decoding algorithm. While the necessary multiplication operations are confined to sign multiplication within the OMS algorithm as stated in (17), rendering them negligible in terms of overall complexity. However, search operations inside (17) are needed to determine two minimum absolute value of the edges in each row of the layer for determining min1 requires $\binom{\theta_i}{1}$ search operations, while determining min2 requires $\binom{\theta_i - 1}{1}$ search operations. Here, θ_i refers to the number of edges (the elements have one value) in each row of the ith layer, where the layers of the 5G NR-LDPC codes have the same number of rows (Z) and each layer has a specific number of edges θ_i, which is the same for all its rows. So, the complexity of the decoder can be calculated by

$$I_m Z \sum_{i=1}^{\lambda} \binom{\Theta_i}{1} + \binom{\Theta_i - 1}{1} \quad (36)$$

where i refers to the layer index and λ refers to number of affected layers, which can be calculate as follows: $\lambda = \left((E + n_f)/Z\right) - 20$ for BG1 and $\lambda = \left((E + n_f)/Z\right) - 8$ for BG2.

Consequently, the proposed system's complexity can be represented by

$$O_{\text{NR-LDPC-GJSTIM-DCSK}} = O_{\text{GJSTIM}} + I_m Z \sum_{i=1}^{\lambda} \binom{\Theta_i}{1} + \binom{\Theta_i - 1}{1} \quad (37)$$

Table II shows that the proposed system complexity increases with the transmitted codeword length. This is primarily due to the increased number of edges, which, in turn, leads to a higher number of search operations. While the codeword length of 7648 demonstrates higher complexity, it achieves Coding gains better than other lengths at a BER of 10^{-3}. In summary, there is a trade-off between the system's complexity and its significantly improved performance, specifically regarding the bit error rate.

TABLE II: THE COMPLEXITY OF THE 5G NR-LDPC-GJSTIM-DCSK PER TRANSMITTED BITS FOR DIFFERENT CODEWORD LENGTHS COMPARED WITH THE UNCODED GJSTIM-DCSK SYSTEM AT R= 1/3 AND β=256

Codeword length E	O_{GJSTIM} per transmitted bits	$O_{NR-LDPC-GJSTIM-DCSK}$ Per transmitted bits	Coding gain under AWGN channel [dB]	Coding gain under Rayleigh fading channel [dB]
3000	63.5641	796.8974	8.85	14
5000	63.5641	1265.1	9.05	16
7648	63.5641	1868.7	9.35	17

VII. CONCLUSIONS

This paper presents the 5G NR-LDPC Codes Based Generalized Joint Subcarrier-Time Index Modulation DCSK System (5G NR-LDPC-GJSTIM-DCSK). The proposed system utilizes 5G NR-LDPC codes for channel coding to improve data transmission reliability and enhance its Bit Error Rate (BER) performance under AWGN and multipath Rayleigh fading channels, thereby offering a significant improvement over the uncoded GJSTIM-DCSK system.

Additionally, this paper employs a method that converts the recovered index bits from the demodulation process into soft form making them suitable as inputs to the decoder. The proposed system performance was evaluated under AWGN and Rayleigh fading channel conditions and contrasted with the uncoded system.

The system exhibited a substantial and evident enhancement in performance, especially with increased codeword lengths, which, however, comes with a rise in system complexity.

Additionally, the study showed that a higher spreading factor degrades the proposed system's performance, and the best system performance was achieved with a code rate of 1/5, yielding coding gains of approximately 11.6 dB over AWGN and 22.2 dB over a Rayleigh fading channel.

Additionally, the performance of the proposed system was compared to that of other coded index modulation DCSK systems, and the results demonstrated the system's robust performance compared to other systems under both Rayleigh fading and AWGN channels.

Ultimately, our proposed system demonstrated robust performance, establishing a strong foundation for future investigations. Further work could involve comparing its performance against Polar codes, particularly considering their distinct roles and strengths within 5G NR.

The proposed system holds great promise for applications requiring high data reliability and efficiency, particularly within the Internet of Things (IoT) and Wireless Sensor Networks (WSNs). Its improved BER performance and robustness make it well-suited for data acquisition and reliable communication in these demanding environments.

CONFLICT OF INTEREST

The authors declare no conflict of interest.

AUTHOR CONTRIBUTIONS

Muntaha K. Musa performed conceptualization, methodology, software, formal analysis, resources, data curation, and writing—original draft preparation. Fadhil S. Hasan assumed the role of supervision, performed a comprehensive work review, and conducted the process of validation. All authors had approved the final version.

ACKNOWLEDGMENT

This work was supported by the Mustansiriyah University, College of Engineering.

REFERENCES

[1] G. Kolumban, B. Vizvari, W. Schwarz, and A. Abel, "Differential chaos shift keying: A robust coding for chaos communication," in *Proc. NDES*, 1996, vol. 96, pp. 87–92.

[2] G. Kaddoum and F. Gagnon, "Design of a high-data-rate differential chaos-shift keying system," *IEEE Trans. Circuits Syst. II, Exp. Briefs*, vol. 59, no. 7, pp. 448–452, Jun. 2012.

[3] G. Kaddoum, E. Soujeri, C. Arcila, and K. Eshteiwi, "I-DCSK: An improved noncoherent communication system architecture," *IEEE Trans. Circuits Syst. II, Exp. Briefs*, vol. 62, no. 9, pp. 901–905, May 2015.

[4] L. Wang, G. Cai, and G. R. Chen, "Design and performance analysis of a new multiresolution M-ary differential chaos shift keying communication system," *IEEE Trans. on Wireless Communications*, vol. 14, no. 9, pp. 5197–5208, May 2015.

[5] G. Cai, Y. Fang, G. Han, F. C. M. Lau, and L. Wang, "A square-constellation-based M-Ary DCSK communication system," *IEEE Access*, vol. 4, pp. 6295–6303, Jan. 2016.

[6] Y. Lu, M. Miao, L. Wang, and W. Xu, "A multilevel code-shifted differential chaos shift keying system with reference diversity," *IEEE Trans. on Circuits and Systems II: Express Briefs*, vol. 67, no. 11, pp. 2462–2466, Jan. 2020.

[7] M. L. Mohammed and F. S. Hasan, "Design and performance analysis of frequency hopping OFDM based noise reduction DCSK system," *Bulletin of Electrical Engineering and Informatics*, vol. 11, no. 3, pp. 1438–1448, Jun. 2022.

[8] F. S. Hasan, "Design and analysis of grouping subcarrier index modulation for differential chaos shift keying communication system," *Physical Communication*, vol. 47, art no. 101325, Mar. 2021.

[9] Y. Tao, Y. Fang, and H. Ma, "Multi-carrier DCSK with hybrid

index modulation: A new perspective on frequency-index-aided chaotic communication," *IEEE Trans. on Communications*, vol. 70, no. 6, pp. 3760–3773, Jun. 2022.
[10] Y. Fang, J. Zhuo, H. Ma, S. Mumtaz, and Y. Li, "Design and analysis of a new index-modulation-aided DCSK system with frequency-and-time resources," *IEEE Trans. on Vehicular Technology*, vol. 72, no. 6, pp. 7411–7425, Jan. 2023.
[11] B. Nazar and F. S. Hasan, "Joint grouping subcarrier and permutation index modulations based differential chaos shift keying system," *Physical Communication*, vol. 61, 102213, Dec. 2023.
[12] R. Abdulkareem and F. S. Hasan, "Design and analysis of grouping non-active frequency -time index modulation for differential chaos shift keying communication system," *International Journal of Intelligent Engineering and Systems*, vol. 17, no. 3, pp. 744–757, May 2024.
[13] R. A. Yaseen and F. S. Hasan, "Design and analysis of grouping active subcarrier frequency-time index modulation for differential chaos shift keying communication system," *Journal of Communications Software and Systems*, vol. 20, no. 2, pp. 173–185, Jan. 2024.
[14] M. K. Musa and F. S. Hasan, "Generalized joint subcarrier-time index modulation aided differential chaos shift keying system," *International Journal of Intelligent Engineering and Systems*, vol. 18, no. 2, pp. 335–356, Mar. 2025.
[15] F. S. Hasan and A. A. Valenzuela, "Joint subcarrier time reference index modulation aided differential chaos shift keying communication system," *IEEE Access*, vol. 12, pp. 159935–159951, 2024.
[16] G. Zhang, X. Wu, Y. Yang, and S. Shao, "Design and analysis of high data rate four-dimensional index modulation for differential chaos shift keying system," *IEEE Trans. on Wireless Communications*, vol. 23, no. 9, pp. 12455–12468, Apr. 2024.
[17] F. S. Hasan, "Design and analysis of grouping five-dimensional index modulation for high data rate DCSK communication system," *Digital Signal Processing*, vol. 163, 105211, Aug. 2025.
[18] Q. Chen, L. Shi, Y. Fang, G. Cai, L. Wang, and G. Chen, "A coded DCSK modulation system over rayleigh fading channels," *IEEE Trans. on Communications*, vol. 66, no. 9, pp. 3930–3942, Sept. 2018.
[19] M. Mosleh, F. S. Hasan, and A. Abdulhameed, "Enhancement of differential chaos shift keying communication system based on LDPC codes," in *Proc. the 1st International Multi-Disciplinary Conference Theme: Sustainable Development and Smart Planning,* 2020. http://dx.doi.org/10.4108/eai.28-6-2020.2297915.
[20] M. F. Mosleh, F. S. Hasan, and A. H. Abdulhameed, "Reduce the resources utilization of LDPC decoder based on min-sum decoder for spread spectrum applications," *IOP Conference Series: Materials Science and Engineering*, vol. 1105, no. 1, 012033, 2021.
[21] Z. Xu, Q. Chen, Y. Li, G. Cai, L. Lin, J. Zheng, and Y. Sun, "Designing protograph LDPC codes for differential chaotic bit-interleaved coded modulation system for underwater acoustic communications," *Journal of Marine Science and Engineering*, vol. 11, no. 5, 914, 2023.
[22] Y. Li, L. Dai, and L. Lv, "Design of an improved M-Ary DCSK-aided protograph-coded communication system," *IEEE Access*, vol. 11, pp. 55002–55010, 2023.
[23] A. Al-Askery, F. Hasan, and A. Thabit, "Investigating the performance of coded GSIM DCSK communication systems over multipath rayleigh fading channel," *Journal of Communications Software and Systems*, vol. 20, no. 4, pp. 298–306, Dec. 2024.
[24] N. Andreadou, F.-N. Pavlidou, S. Papaharalabos, and P. T. Mathiopoulos, "Quasi-Cyclic Low-Density Parity-Check (QC-LDPC) codes for deep space and high data rate applications," in *Proc. the International Workshop on Satellite and Space Communications*, Siena, Italy, 2009, pp. 225–229.
[25] 3GPP Organizational Partners, 3rd Generation Partnership Project; Technical Specification Group Radio Access Network, NR; Multiplexing and Channel Coding, 2022, pp. 22–39.
[26] T. T. B. Nguyen, T. N. Tan, and H. Lee, "Efficient QC-LDPC encoder for 5G new radio," *Electronics*, vol. 8, no. 6, 668, 2019.
[27] D. E. Hocevar, "A reduced complexity decoder architecture via layered decoding of LDPC codes," in *Proc. the IEEE Workshop on Signal Processing Systems*, SIPS 2004, 2004, pp. 107–112.
[28] J. Chen, R. M. Tanner, C. Jones, and Y. Li, "Improved min-sum decoding algorithms for irregular LDPC codes," in *Proc. the International Symposium on Information Theory*, ISIT 2005, Adelaide, SA, Australia, 2005, pp. 449–453.
[29] Y. Ren, H. Harb, Y. Shen, A. Balatsoukas-Stimming, and A. Burg, "A generalized adjusted min-sum decoder for 5G LDPC codes: Algorithm and implementation*," IEEE Trans. on Circuits and Systems I: Regular Papers*, vol. 71, no. 6, pp. 2911–2924, Jun. 2024.

Muntaha K. Musa was born in Baghdad, Iraq in 1986. She received her B.Sc. degree in communication and electronic engineering from University of Baghdad, Iraq in, 2008. She is currently pursuing an M.Sc. degree in electronic and communication engineering at Al-Mustansiriyah University. Her research interests include Wireless Communication Systems, Index Modulation, and ChaoticModulation.

Fadhil S. Hasan was born in Baghdad, Iraq in 1978. He received his B.Sc. degree in electrical engineering in 2000 and his M.Sc. degree in electronics and communication engineering in 2003, both from the Mustansiriyah University, Iraq. He received Ph.D. degree in 2013 in Electronics and Communication Engineering from the Basrah University, Iraq. In 2005, he joined the Faculty of Engineering at the Mustansiriyah University in Baghdad. His recent research activities are Wireless Communication Systems, Multicarrier System, Wavelet based OFDM, MIMO System, Speech and Image Signal Processing, Chaotic Cryptography, Chaotic Modulation, FPGA and Xilinx System Generator based Communication System. Now he has been a Prof. at the Mustansiriyah University, Iraq.